crystals

MDPI

*Article*

# Study on Creep Properties of Al-Zn-Mg-Cu Alloys

**Wen Zhang [1] and Yunhai Su [2,*]**

[1] Siegnata Automotive Control Systems (Shenyang) Co., Ltd., Shenyang 110141, China; eric.zhangwen@outlook.com
[2] School of Materials Science and Engineering, Shenyang University of Technology, Shenyang 110870, China
* Correspondence: su_yunhai@sut.edu.cn; Tel.: +86-13709840941

**Abstract:** This article conducts high-temperature creep tests on an Al-6.5Zn-2.3Mg-2.5Cu-0.1Zr-0.2Sc alloy in a solid solution + aging state at 200 °C and 150–180 MPa. Characterization of the microstructure of the specimen after creep test fracture was performed using SEM and TEM. The results indicate that the steady-state creep rate range of the alloy was $10^{-9}$ to $10^{-8}$ $s^{-1}$, which was positively correlated with applied stress, while the creep life was negatively correlated with applied stress. Through failure analysis, it was found that the main deformation mechanism of the alloy was the dislocation climbing mechanism. The fracture mode of the alloy was ductile fracture.

**Keywords:** Al-6.5Zn-2.3Mg-2.5Cu-0.1Zr-0.2Sc alloy; solution and aging; creep; fracture mode

## 1. Introduction

Al and Al alloys are widely used in industrial fields such as automotive manufacturing, mechanical manufacturing, aerospace, shipbuilding, and construction due to their high specific stiffnesses and strengths, low densities, and good tensile strengths. Currently, Al alloys are one of the most widely used lightweight structural material [1]. A high-strength and high toughness Al alloy with Zn as the main alloying element and a small amount of Mg and Cu added, a seven-series Al alloy, can achieve high strength, hardness, and good fatigue-cycle resistance after heat treatment. Common grades such as 7075 and 7050 are widely used in structural parts such as aircraft mounts, crossbeams, aircraft skins, and landing gears [2].

An Al alloy ingot after casting has severe intergranular segregation, and the internal stress of the alloy cannot be eliminated, resulting in various properties of the alloy generally failing to meet standards. Homogenization treatment of an alloy refers to the process of holding the alloy at a solid solution line or eutectic temperature for a period of time through heating, allowing the segregated phase to dissolve back into the matrix to form a supersaturated solid solution and a small amount of dispersed fine precipitates. The microstructure and mechanical properties of the alloy after homogenization treatment are significantly improved. In addition, the melting point of Zr added is around 1850 °C, which is significantly different from that of Al. During the solidification process, Zr is easily enriched in dendrites and forms segregation. Homogenization treatment can make $Al_3Zr$ particles uniformly and dispersedly precipitate in the matrix, reducing the width of the precipitation-free zone [3]. The heat-treatment strengthening of an Al-Zn-Mg-Cu alloy mainly relies on the type and quantity of precipitates during the aging process. Solid-solution treatment is to heat the alloy to a high-temperature single-phase zone and maintain a constant temperature for a period of time, so that the excess phase is fully dissolved in the solid solution and quickly cooled, thereby obtaining a supersaturated solid solution. The higher the supersaturation of the solid solution in the matrix, the more precipitated phases during the aging process, and the higher the strength of the alloy. The factors that affect the effectiveness of solid solution treatment mainly include the solution temperature, solution time, and cooling temperature. Generally speaking, the higher the solution temperature,

check for updates

**Citation:** Zhang, W.; Su, Y. Study on Creep Properties of Al-Zn-Mg-Cu Alloys. *Crystals* **2023**, *13*, 1554. https://doi.org/10.3390/cryst13111554

Academic Editor: José L. García

Received: 11 October 2023
Revised: 20 October 2023
Accepted: 25 October 2023
Published: 30 October 2023

the more strengthening phases dissolve into the matrix, and the better the effect of the subsequent aging treatment. However, an excessive solution temperature can cause alloy-grain growth, promote recrystallization, and lead to an overburning phenomenon [4–6].

Srivastava et al. [7] studied the high-temperature creep behavior of 7075 high-strength aluminum alloy at a creep temperature of 350–410 °C and a creep stress of 1.8–6.3 MPa. The results indicate that the creep rate of the alloy under low stress conforms to the Nabarro Herring theory. Peng et al. [8] conducted creep tests on Al-Cu-Mg-Ag alloys with different Cu contents to investigate the effects of creep test temperature and applied stress on the creep behavior of the alloy. The experiment shows that keeping the stress constant and increasing the test temperature significantly increases the steady-state creep rate of the alloy compared to increasing the applied stress while keeping the temperature constant. Under this experimental condition, the creep mechanism of the Al-Cu-Mg-Ag alloy is dislocation climbing. Lin et al. [9] studied the creep behavior of an Al-Cu-Mg alloy at temperatures ranging from 200 to 350 °C, and found that creep temperature and stress have a significant impact on the fracture behavior of the alloy. In addition, Xu et al. [10] focused on the nonisothermal creep deformation behavior of an Al-Cu-Mg alloy and found that the creep stain at the heating stage is 22.28–26.86% of the total creep strain. Xu et al. [11] studied the creep aging behavior of Al-Cu-Mg alloy at different heating rates and found that the creep deformation at the heating stage is decreased with increasing heating rates.

An Al-Zn-Mg-Cu alloy is used as an aircraft body skin and some structural components. During flight, the temperature of the structural components can reach 150 °C, and in special cases, even exceed 200 °C [12]. Previous studies mainly conducted creep testing under a wide range of temperature and stress conditions, but there have been few reports on creep testing in the smaller temperature and stress range described in this article. Therefore, this article mainly conducts creep testing on T6-state Al-Zn-Mg-Cu alloy under conditions of 200 °C and 150–180 MPa. We provide a theoretical basis for the application of T6-state Al-Zn-Mg-Cu alloy in aircraft.

## 2. Experimental Materials and Methods

### *2.1. Test Materials*

The experimental material was selected as an Al-Zn-Mg-Cu-Zr-Sc alloy after extrusion. Measurement of its element content was performed using the chemical analysis method, as shown in Table 1. The smelting raw materials were 99.96% industrial pure aluminum, 99.8% industrial pure zinc, 99.90% copper block, 99.91% magnesium block, and intermediate alloys of Al-5% Zr and Al-2% Sc. The mechanical properties obtained from the tensile testing of the alloy are shown in Table 2.

**Table 1.** Chemical compositions of the alloy (wt.%).

| Element | Zn | Mg | Cu | Zr | Sc | Al |
|---|---|---|---|---|---|---|
| Content | 7.0 | 2.5 | 2.0 | 0.1 | 0.2 | Bal. |

**Table 2.** Tensile mechanical properties of the material.

| Aging time (h) | 10 | 16 | 22 | 28 | 34 |
|---|---|---|---|---|---|
| Tensile strength (MPa) | 612 | 667 | 723 | 668 | 648 |
| Yield strength (MPa) | 476 | 524 | 551 | 534 | 489 |

### *2.2. Heat Treatment*

To perform solid solution and aging treatment on the rod-shaped material Al-Zn-Mg-Cu aluminum alloy, the SX-4-10 box-type resistance furnace was first heated to 470 °C. After reaching the temperature, the sample was placed for 2 h of insulation, and then taken out and quenched in water. This step is called solid-solution treatment. The aging treatment temperature was selected as 120 °C, with a duration of 1 h, 10 h, 22 h, 34 h and air cooling.

### *2.3. Creep Experiment*

Creep tests were conducted on an SRD-100 microcomputer-controlled electronic creep testing machine (Nanjing Times Testing Equipment Co., Ltd., Nanjing, China), according to the GB/T2039-2008 standard. The specific operations are as follows: the creep properties were tested on a GTW504 creep testing machine (Tektronix, Oregon, America). The testing temperature is 200 °C, and the stress range is 150–180 MPa until the specimen is stretched to fracture. During long-term creep, the radial temperature difference of the sample did not exceed ±2 °C. At least two parallel samples were used for each creep test condition, and all mechanical properties were the average values of the measured parameters under the same experimental conditions. The shape and size of the creep specimen are shown in Figure 1.

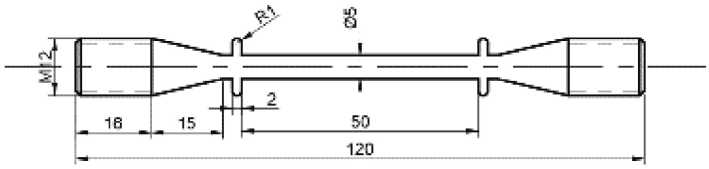


**Figure 1.** Creep specimen shape and size (mm).

### *2.4. Observation of Microstructure*

We observed and analyzed the metallographic microstructure of alloy samples in different states using a HYZX-2000 metallographic microscope (Laizhou Laiyi Test Instrument Co., Ltd., Laizhou, China). The samples were polished sequentially with 400 #, 800 #, 1000 #, 1500 #, and 2000 # silicon carbide (SiC) paper, and were ground using an MC004-M-2 metallographic (Shanghai Yanrun Light Machinery Technology Co., Ltd., Shanghai, China) sample pre grinding machine. Afterwards, we used a WX100 polishing machine (Shenzhen Pilot Huanyu Technology Co. Ltd., Shenzhen, China) to polish the surface of the sample, wiped it clean with alcohol, and then blow dried it. We used Keller corrosion solution (2.5% $HNO_3$ + 1.5% HCl + 0.5% HF + 95.5% $H_2O$) for corrosion to observe the microstructure.

The fracture morphology of the tensile, fatigue, and creep fracture specimens was observed using an S-3400N scanning electron microscope (HITACHI, Tokyo, Japan) to determine the fracture mode of the Al alloy under experimental conditions.

A JEM-2100 transmission electron (JEOL, Tokyo, Japan) microscope was used to observe the microstructure of the alloy, the size, morphology, distribution, etc., of its precipitates, and observe the dislocations near the fracture surface in order to analyze and determine the deformation mechanism of the alloy. The sample preparation process for scanning electron microscopy observation is as follows: Firstly, the sample is processed into 0.5 mm thin slices using a cutting machine, and then manually thinned to about 100 μm on metallographic sandpaper before punching into φ3 mm circular slices. The specimens are thinned and perforated, performed using a TenuPol-5 dual jet thinner, with the electrolyte 25% $HNO_3$ + 75% $CH_3OH$, with a double jet temperature of about −25 °C and a voltage of about 19 V. The sample was rinsed with water after perforation and then washed twice with alcohol.

## 3. Experimental Results

### *3.1. Creep Results*

The creep curves of the Al-6.5Zn-2.3Mg-2.5Cu-0.1Zr-0.2Sc alloys in different aging states are shown in Figure 2 when subjected to stresses of 150 MPa, 160 MPa, 170 MPa, and 180 MPa at 200 °C. Figure 2a shows the creep strain–time relationship curve of an alloy aged for 22 h under conditions of 200 °C and 150–180 MPa. Observing the curve in the figure, it can be seen that the alloy underwent three stages, initial creep, steady creep, and accelerated creep, under various stress conditions. However, at 180 MPa, the steady-state creep stage of the alloy was relatively short. Figure 2b shows the creep strain–time relationship curve of the 34 h aged alloy at 200 °C and 150–180 MPa, which was consistent with the 22 h aged

sample. Compared to the 22 h aged alloy exhibiting a shorter steady-state creep stage at 180 MPa, the 34 h aged alloy exhibited almost no steady-state creep stage at 180 MPa.

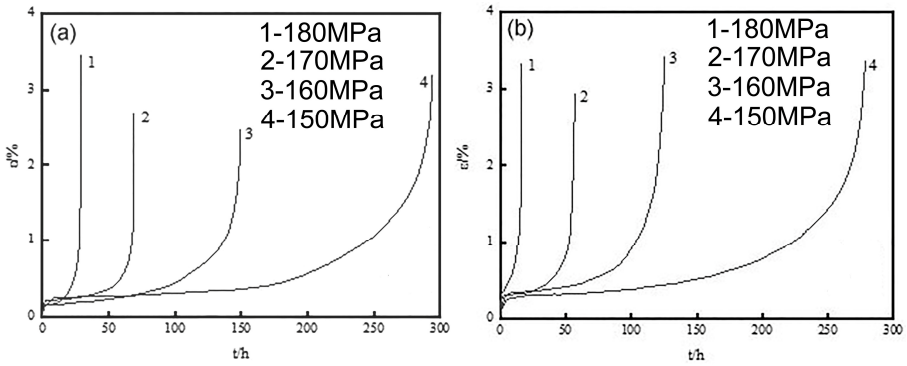


**Figure 2.** Creep curve of time-efficient Al-6.5Zn-2.3Mg-2.5Cu-0.1Zr-0.2Sc alloy at different stresses at 200 °C. (**a**) aging 22 h, (**b**) aging 34 h.

In creep testing, the creep rate of alloys is usually characterized by the ratio of creep strain to creep time. By calculating the slopes of the curves of the two aged alloys under different stresses in Figure 2, it can be found that the slopes of the creep curves of both the aged alloys decreased with an increase in creep time during the initial creep stage. When the alloy entered the steady-state creep stage, the slope of the creep curve remained basically unchanged; as the creep time continued to increase, the alloy entered the accelerated creep stage, and the slopes of the creep curves of both the aged alloys rapidly increased until the alloy fractured. Comparing the creep curves of the 22 h and 34 h aged alloys, it was found that when the same external stress was applied to the alloy, the slope of the 22 h aged alloy was smaller. Overall, the creep life of the aged Al-6.5Zn-2.3Mg-2.5Cu-0.1Zr-0.2Sc alloy decreased with the increase in applied stress.

Linear fitting is performed on the steady-state creep stage of the creep curve under different creep test conditions to obtain the corresponding steady-state creep rate. The steady-state creep rates of the T6 Al-6.5Zn-2.3Mg-2.5Cu-0.1Zr-0.2Sc alloy in the range of 200 °C and 150–180 MPa are shown in Table 3.

**Table 3.** Steady-state creep rate of time-sensitive Al-6.5Zn-2.3Mg-2.5Cu-0.1Zr-0.2Sc alloy at different stresses at 200 °C.

| Aging Time | σ (MPa) | $\dot{\varepsilon}$ ($s^{-1}$) |
|---|---|---|
| 22 h | 150 | $2.55 \times 10^{-9}$ |
| | 160 | $4.39 \times 10^{-9}$ |
| | 170 | $8.16 \times 10^{-9}$ |
| | 180 | $3.16 \times 10^{-8}$ |
| 34 h | 150 | $2.64 \times 10^{-9}$ |
| | 160 | $5.42 \times 10^{-9}$ |
| | 170 | $1.66 \times 10^{-8}$ |
| | 180 | $5.11 \times 10^{-8}$ |

The rate of T6-state Al-6.5Zn-2.3Mg-2.5Cu-0.1Zr-0.2Sc in the steady-state creep stage is related to the creep temperature (T) and stress (σ), and the relationship can be expressed by the creep constitutive equation [13]:

$$\dot{\varepsilon} = A\sigma^n exp\left(-\frac{Q}{RT}\right) \quad (1)$$

Among them, $\dot{\varepsilon}$ is the steady-state creep rate, $A$ is a constant, $n$ is the apparent stress index, $Q$ is the activation energy of creep behavior, and $R$ is the molar gas constant

(8.314 $Jmol^{-1}K^{-1}$). By taking the logarithm of each end of the formula and simplifying it, we can obtain

$$\ln \dot{\varepsilon} = n \ln \sigma + \ln A - \frac{Q}{R} \times \frac{1}{T} \quad (2)$$

According to Formula (1), when the creep temperature remains constant, $\ln \dot{\varepsilon}$ and $\ln \sigma$ have a linear relationship. Draw a $\ln \dot{\varepsilon} - \ln \sigma$ curve based on the data in Table 3 and perform linear fitting. The slope in the $\ln \dot{\varepsilon} - \ln \sigma$ relationship curves is n, and the intercept is the constant.

The double logarithmic relationship curve between the creep rate and stress during the steady-state creep of the Al-6.5Zn-2.3Mg-2.5Cu-0.1Zr-0.2Sc alloy in different effective states, at 200 °C and a stress of 150–180 MPa, is shown in Figure 3. By fitting the creep rate and stress data, it can be concluded that when aged for 22 h, its $n$ = 13.33 and C = −73.99. When the aging time was 34 h, its $n$ = 16.42 and C = −89.42. Therefore, it can be determined that the relationship between the creep rate and applied stress durin g the steady-state creep of Al-6.5Zn-2.3Mg-2.5Cu-0.1Zr-0.2Sc alloy with different aging times in the range of 200 °C and 150–180 MPa is as follows:

$$\dot{\varepsilon}1 = 7.35 \times 10^{-33} \sigma^{13.33} \quad (3)$$

$$\dot{\varepsilon}2 = 1.46 \times 10^{-39} \sigma^{16.42} \quad (4)$$

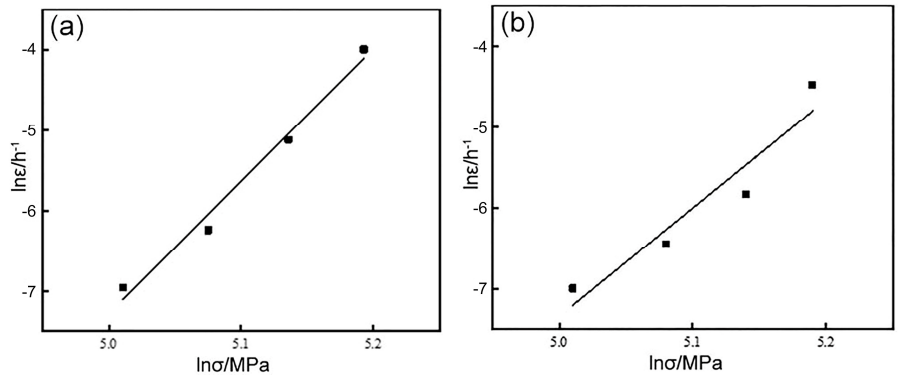


**Figure 3.** Dual logarithmic curve of steady-state creep rate and stress of non-simultaneously active Al-6.5Zn-2.3Mg-2.5Cu-0.1Zr-0.2Sc alloy at 200 °C. (**a**) Aging for 22 h, and (**b**) aging for 34 h.

Among them, Formulas (3) and (4), respectively, represent the relationship between the steady-state rate and applied stress of the alloy aged for 22 h and 34 h.

Table 4 presents the creep test data of the T6 Al-6.5Zn-2.3Mg-2.5Cu-0.1Zr-0.2Sc alloy at 200 °C and 150–180 MPa. It can be found that the creep life of the Al-6.5Zn-2.3Mg-2.5Cu-0.1Zr-0.2Sc alloy in different heat treatment states decreased with an increase in applied stress, while its steady-state creep rate increased with the applied stress. Under a stress of 150 MPa, the steady-state creep rate of the alloy aged for 22 h was 2.55 × $10^{-9}$ $s^{-1}$, and its creep life was 293 h; the steady-state creep rate of the 34 h aged alloy was 2.64 × $10^{-9}$ $s^{-1}$, and its creep life was 280 h. Under this stress condition, the creep life of the two aged alloys differed by 4.6%. Under a stress of 160 MPa, the steady-state creep rate of the alloy aged for 22 h was 4.39 × $10^{-9}$ $s^{-1}$, and the creep life was 148 h. The steady-state creep rate of the aged 34 h alloy was 5.42 × $10^{-9}$ $s^{-1}$, and the creep life was 125 h. As the stress continued to increase to 170 MPa, the life of the 22 h aged alloy decreased to 68 h, and its steady-state creep rate increased to 8.16 × $10^{-9}$ $s^{-1}$. The service life of the 34 h aged alloy was shortened to 57 h, and its steady-state creep rate was 1.66 × $10^{-8}$ $s^{-1}$. When the stress increased to 180 MPa, the creep life of the alloy was significantly shortened. The creep life of the 22 h aged alloy was only 29 h, and the steady-state creep rate was 3 to $10^{-8}$ $s^{-1}$. However, the creep life of the 34 h aged alloy was 16 h, and the steady-state creep rate was $1^{-10}$ to 8 $s^{-1}$.

At this time, the life of the two aged alloys was about twice that. The experimental results show that the T6-state Al-6.5Zn-2.3Mg-2.5Cu-0.1Zr-0.2Sc alloy is very sensitive to stress changes, so that under high external stress, the alloy quickly enters the third stage until fracture after undergoing a brief steady-state creep stage. Under low-stress conditions, the difference in creep life between the two aged alloys is relatively small. However, with the increase in creep applied stress, the life of the two aged alloys not only shortens but also the relative life difference becomes larger.

**Table 4.** T6-state Al-6.5Zn-2.3Mg-2.5Cu-0.1Zr-0.2Sc alloy creep test data.

| Aging Time | σ (MPa) | t (h) |
|---|---|---|
| 22 h | 150 | 293 |
| | 160 | 148 |
| | 170 | 68 |
| | 180 | 29 |
| 34 h | 150 | 280 |
| | 160 | 125 |
| | 170 | 57 |
| | 180 | 16 |

### *3.2. Creep Life*

The double logarithmic curve of the creep-fracture life and steady-state creep rate of the T6-state Al-6.5Zn-2.3Mg-2.5Cu-0.1Zr-0.2Sc alloy is shown in Figure 4. It can be seen that the double logarithmic curves of the creep fracture time and steady-state creep rate of the two aged alloys have a linear relationship, and the creep life follows the Monkman–Grant relationship. The Monkman–Grant [14] relationship is as follows:

$$(\dot{\varepsilon})^{\beta} t_f = C_{MG} \tag{5}$$

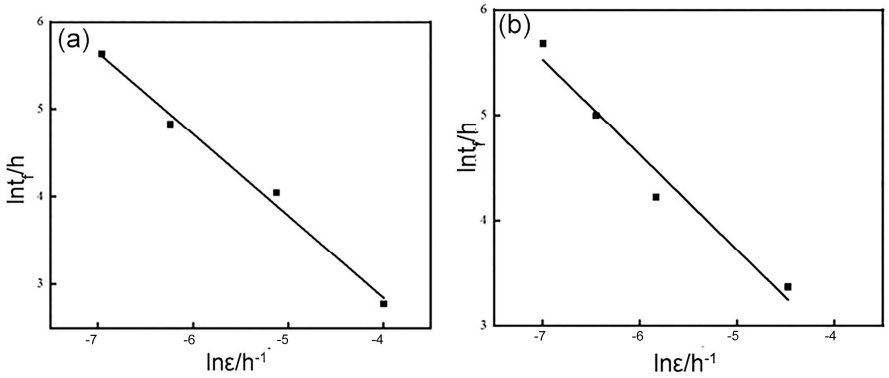


**Figure 4.** Double logarithmic curve of creep life and steady-state creep rate of solid-solution + time-efficient Al-6.5Zn-2.3Mg-2.5Cu-0.1Zr-0.2Sc alloy at 200 °C. (**a**) Aging for 22 h, and (**b**) aging for 34 h.

Among them, $\dot{\varepsilon}$ is the steady-state creep rate, $t_f$ is the fracture time, and $C_{MG}$ is related to the material and test temperature, and taking the logarithm of the above equation, we obtain

$$\beta \ln \dot{\varepsilon} + \ln t_f = \ln C \tag{6}$$

From this, it can be concluded that

$$\ln t_f = \ln C - \beta \ln \dot{\varepsilon} \tag{7}$$

where $\beta$ is the slope of the double logarithmic curve. By fitting the double logarithmic curves of fracture time and steady-state creep rate, it can be found that the slope of the 22 h aged alloy curve was −0.903 and the intercept was −0.798, while the slope of the 34 h aged alloy curve was −0.934 and the intercept was −0.892. The relationship between the creep life and rate of the T6-state alloy can be obtained as follows:

$$t_f = 0.405\dot{\varepsilon}^{-0.798} \tag{8}$$

$$t_f = 0.393\dot{\varepsilon}^{-0.892} \tag{9}$$

According to the relationship between the steady-state creep rate, temperature, and applied stress, the creep fracture time can be expressed as

$$t_f \propto \dot{\varepsilon} = A\sigma^n exp\left(-\frac{Q}{RT}\right) \tag{10}$$

Take the logarithm of both sides of the above equation, which can be expressed as

$$\ln t_f = P \ln \sigma + B \tag{11}$$

Among them, $B$ is a constant and $P$ is the slope of the curve.

Linear fitting of the data in Figure 5 shows that the slope of the 22 h aged alloy curve was −12.743 and the intercept was 69.681, while the slope of the 34 h aging alloy curve was −15.405 and 82.963. The relationship between the creep fracture life and stress was obtained as follows

$$t_f = 1.828 \times 10^{30}\sigma^{-12.743} \tag{12}$$

$$t_f = 1.073 \times 10^{36}\sigma^{-15.405} \tag{13}$$

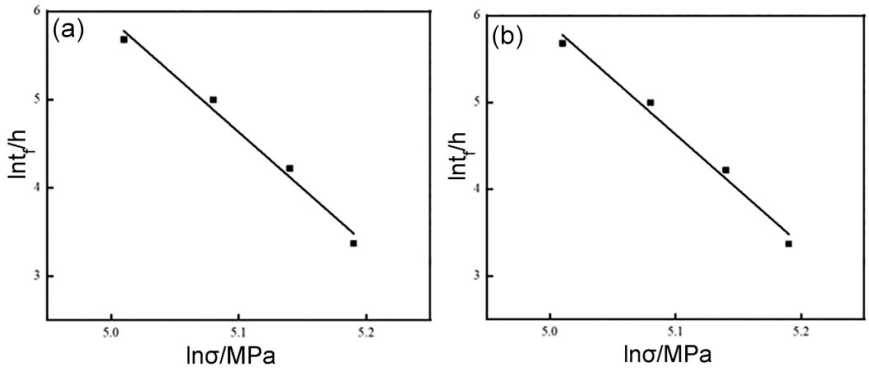


**Figure 5.** Bi-logarithmic curve of creep life and stress of solid-solution + time-efficient Al-6.5Zn-2.3Mg-2.5Cu-0.1Zr-0.2Sc alloy at 200 °C. (**a**) Aging for 22 h, and (**b**) aging for 34 h.

### *3.3. Microstructure after Creep Deformation*

Figure 6 shows the microstructure near the creep fracture surface of the Al-6.5Zn-2.3Mg-2.5Cu-0.1Zr-0.2Sc alloy aged for 22 h at 200 °C under different stresses. Under a creep stress of 150 MPa, the precipitates were small, uniform, and numerous, with a size of approximately 24 nm; when the creep stress was 160 MPa, the precipitates were slightly coarsened, with a size of about 32 nm. When the creep stress increased to 170 MPa, the precipitates underwent significant coarsening, with a size of about 55 nm. When the creep stress increased to 180 MPa, the coarsening degree of the precipitates rapidly increased, with a size of about 73 nm.

Figure 7 shows the microstructure near the creep fracture surface of the Al-6.5Zn-2.3Mg-2.5Cu-0.1Zr-0.2Sc alloy after aging for 34 h under different stresses at 200 °C. Under

a creep stress of 150 MPa, the precipitates in the alloy were small, uniform, and numerous, with a size of approximately 27 nm. When the creep stress was 160 MPa, it can be seen that the precipitates were slightly coarsened, with a size of about 38 nm. When the creep stress increased to 170 MPa, the precipitates in the alloy underwent significant coarsening, with a size of about 62 nm. When the creep stress increased to 180 MPa, the coarsening degree of the precipitates in the alloy rapidly increased, with a size of about 96 nm.

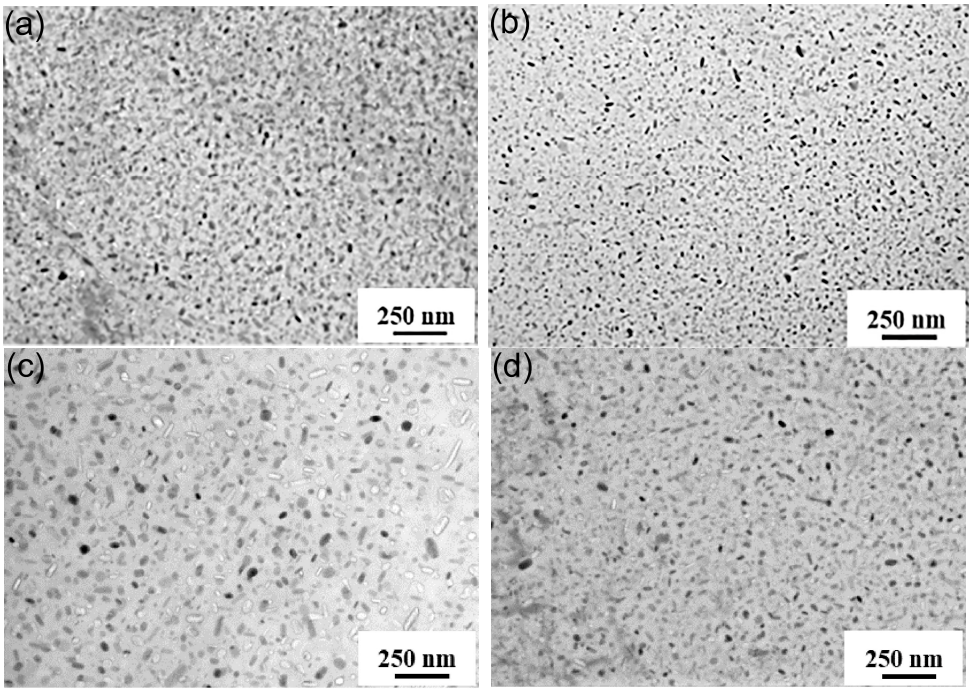


**Figure 6.** Microstructure of Al-6.5Zn-2.3Mg-2.5Cu-0.1Zr-0.2Sc alloy with aging at 200 °C and 22 h under different stresses. (**a**) 150 MPa, (**b**) 160 MPa, (**c**) 170 MPa, and (**d**) 180 MPa.

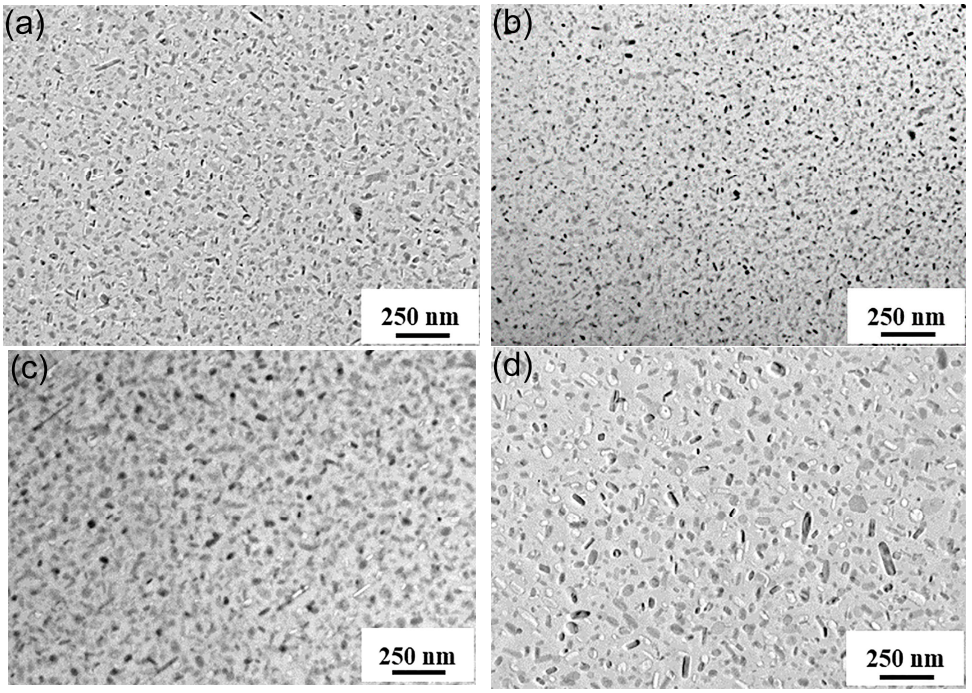


**Figure 7.** Microstructure of Al-6.5Zn-2.3Mg-2.5Cu-0.2.2Sc alloy after creep at 200 °C and aging of 34 h under different stresses. (**a**) 150 MPa, (**b**) 160 MPa, (**c**) 170 MPa, and (**d**) 180 MPa.

Figure 8 shows the morphology of the precipitation-free zones in the creep deformation zone of the T6-state Al-6.5Zn-2.3Mg-2.5Cu-0.1Zr-0.2Sc alloy under different stresses. From the observations of Figure 8a,b, it can be observed that under the action of an external stress of 150 MPa, the width of the precipitate-free zone of the two aged alloys was not significantly different. The width of the precipitate-free zone of the 22 h aged alloy was 53 nm, while the width of the precipitate-free zone of the 34 h aged alloy was about 58 nm. However, compared to 150 MPa, when the applied stress increased to 180 MPa, the width difference of the precipitated phases in the active alloy increased significantly at different times. The width of the precipitate-free zone in the 22 h aged alloy was 83 nm, and the width of the 34 h aged alloy was 117 nm, with a difference of 34 nm between the two.

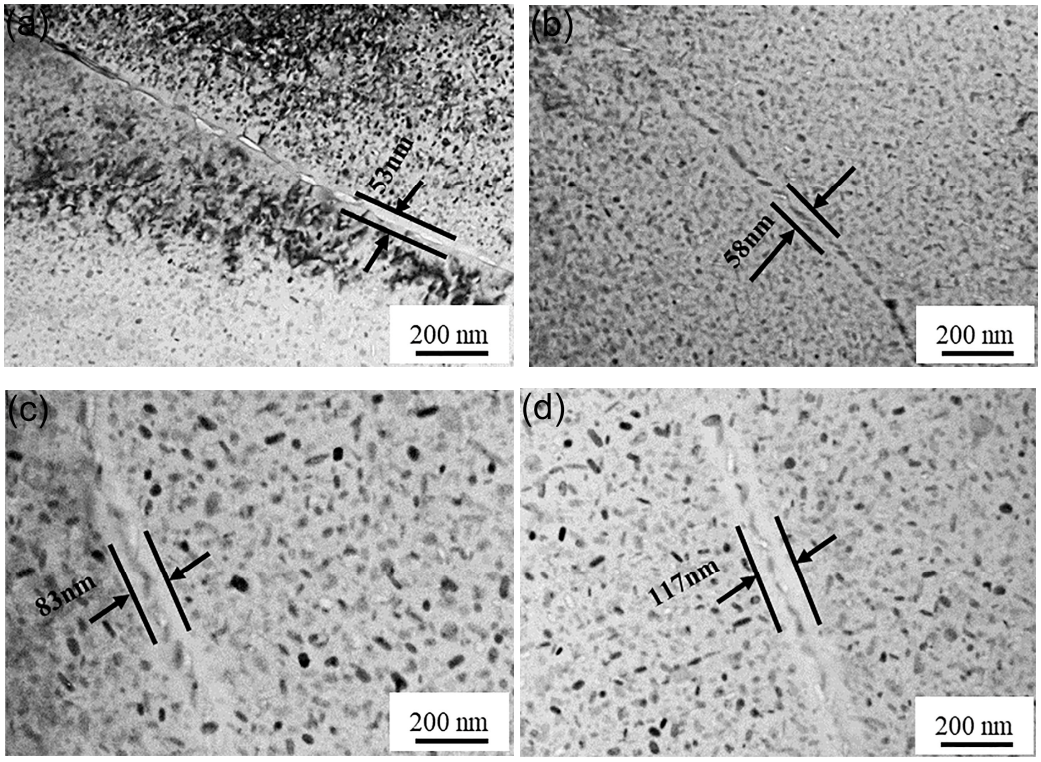


**Figure 8.** Morphology of the creep deformation zone of the Al-6.5Zn-2.3Mg-2.5Cu-0.1Zr-0.2Sc alloy under different stresses. (**a**) After 22 h aging, 150 MPa; (**b**) 34 h aging, 150 MPa; (**c**) 22 h aging, 180 MPa; and (**d**) 34 h aging, 180 MPa.

Figure 9 shows the dislocation entanglement in the creep deformation zone of the aged T6-state Al-6.5Zn-2.3Mg-2.5Cu-0.1Zr-0.2Sc alloy at 200 °C and under different stresses. As shown in the figure, a large amount of dislocation entanglement can be observed in the micro deformation zone of 22 h and 34 h aged alloys at 200 °C under different external stresses.

### *3.4. Creep Fracture Morphology*

Figure 10 shows the creep-fracture SEM morphology of the Al-6.5Zn-2.3Mg-2.5Cu-0.1Zr-0.2Sc alloy treated for 22 h at 200 °C and 150–180 MPa.

Under a stress of 150 MPa, a large number of closely sized dimples can be observed on the creep fracture surface of the alloy, with a large number of precipitate particles and a small number of pores at the bottom of the dimples. Under the condition of applied stress at 160 MPa, the distribution of dimples on the fracture surface of the alloy was uneven, and the size of dimples varied, but there were still many precipitates at the bottom. As the applied stress continued to increase, obvious white tearing edges can be observed on the creep fracture surface of the alloy, and the surface of the fracture became rough and uneven.

Under the condition of 180 MPa, a large number of dimples of different sizes and depths were distributed on the creep fracture surface of the alloy, and the precipitates particles at the bottom of the dimples shed a lot under the action of higher stress.

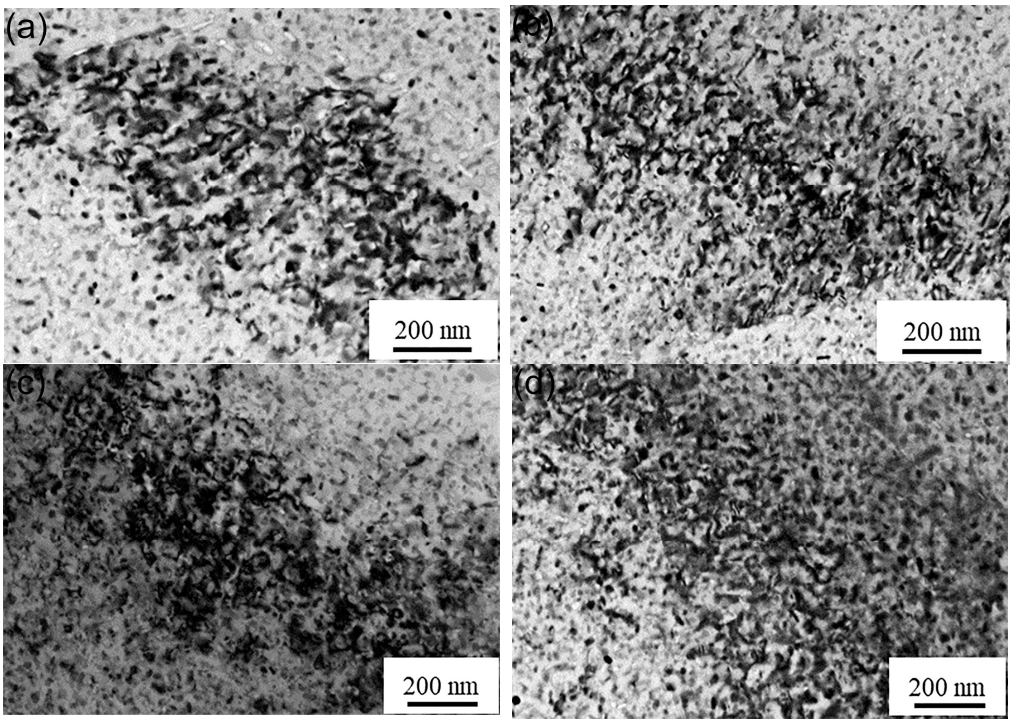


**Figure 9.** Dislocation configuration of the creep deformation zone of the Al-6.5Zn-2.3Mg-2.5Cu-0.1Zr-0.2Sc alloy in the T6 state under different stresses. (**a**) At 22 h aging, 150 MPa; (**b**) 34 h aging, 150 MPa; (**c**) 22 h aging, 180 MPa; and (**d**) 34 h aging, 180 MPa.

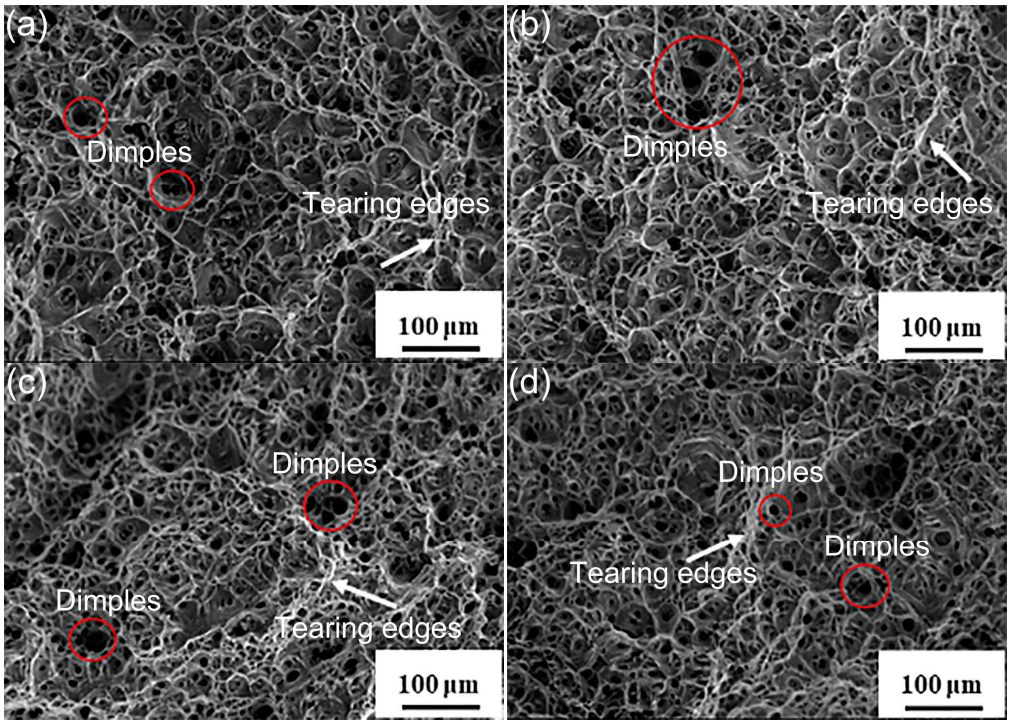


**Figure 10.** Morphology of creep fracture of 22 h aged Al-6.5Zn-2.3Mg-2.5Cu-0.1Zr-0.2Sc alloy at 200 °C and 150–180 MPa. (**a**) 150 MPa, (**b**) 160 MPa, (**c**) 170 MPa, and (**d**) 180 MPa.

Figure 11 shows the creep-fracture SEM morphology of the Al-6.5Zn-2.3Mg-2.5Cu-0.1Zr-0.2Sc alloy after aging for 34 h at 200 °C and 150–180 MPa.

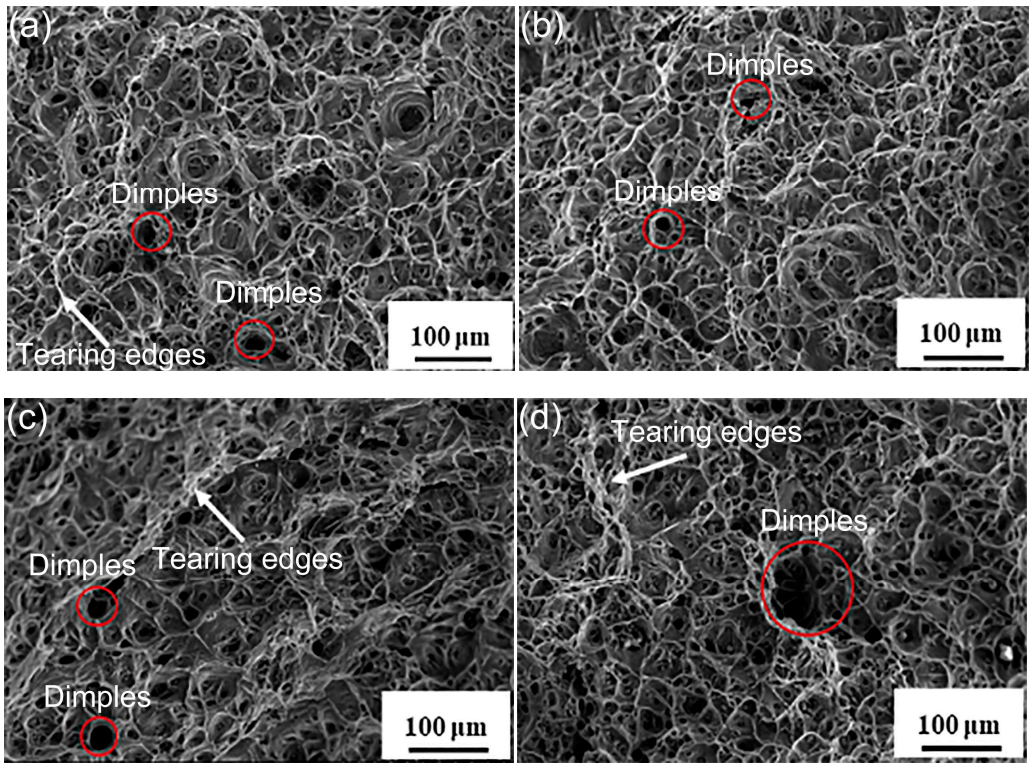


**Figure 11.** Morphology of creep fracture of 34 h aged Al-6.5Zn-2.3Mg-2.5Cu-0.1Zr-0.2Sc alloy at 200 °C and 150–180 MPa. (**a**) 150 MPa, (**b**) 160 MPa, (**c**) 170 MPa, and (**d**) 180 MPa.

The overall composition of the fracture morphology of the 22 h aged alloy was similar, and the creep fracture of the alloy under different external stress conditions also exhibited ductile fracture characteristics. There were a large number of dimples on the fracture surface, accompanied by dimples and bright white tearing edges. However, under the same applied stress conditions, especially under high stress, the fracture morphology of the two aged alloys was slightly different. Compared to aging for 22 h, aging for 34 h resulted in a larger roughness of the fracture surface, more tearing edges, and obvious large pores under the condition of 180 MPa.

## 4. Discussion

The T6-state Al-6.5Zn-2.3Mg-2.5Cu-0.1Zr-0.2Sc alloy undergoes three processes of initial creep, steady-state creep, and accelerated creep under creep conditions of 200 °C and 150–180 MPa. During the initial stage of creep, movable dislocations that are prone to slip in the alloy move under external forces, resulting in a relatively fast creep rate. As the movement of dislocations continues, the precipitates interact with the moving dislocations, hindering their movement, slowing down the creep rate, and the alloy enters the steady-state creep stage. Under the action of external stress, pores are formed inside the alloy, leading to the occurrence of stress concentration. The creep rate of the alloy increases significantly, and the alloy enters the accelerated creep stage until fracture. Under creep conditions of 200 °C and 150–180 MPa, the creep fracture of the Al-6.5Zn-2.3Mg-2.5Cu-0.1Zr-0.2Sc alloy is ductile fracture, and the fracture surface is mainly composed of ductile dimples, tearing edges, and creep pores [15–17]. Under high-temperature conditions, dislocations near grain boundaries are more prone to climbing and causing deformation of the grain boundaries through slip and torsion. The interconnected parts of grain boundaries generally experience stress concentration during the sliding process, which makes it easy for

these parts to preferentially form cracks and evolve into pores. In addition, the formation of creep pores is closely related to the precipitation of alloys. According to the theory of dislocations, dislocation rings are stacked around the precipitates. In the absence of external forces, the dislocation rings maintain an equilibrium state under the combined action of the repulsion of the precipitates and the stacking stress. When the applied external force is large enough, the dislocations that had accumulated near the precipitated phase will move again. When the accumulated elastic strain energy is sufficient to overcome the interfacial bonding force between the precipitated phase and the matrix phase and form a new surface, micro pores will be formed.

The steady-state creep rate often depends on the creep stress. The new and existing dislocations generated during the creep process are hindered by the precipitates during movement, resulting in a decrease in the creep rate; on the other hand, under the combined action of temperature and applied stress, dislocations gain more energy and have stronger mobility, accelerating the creep rate. The two factors work together to ultimately form a steady-state creep stage. At the same time, while other experimental conditions remain unchanged, as the applied stress increases, the driving force of dislocation movement also increases, making it easier for dislocations to cross obstacles, and thus increasing the creep rate [18,19]. For aluminum alloys, the changes in precipitates also have a significant impact on creep behavior. By observing the microstructure of the T6-state Al-6.5Zn-2.3Mg-2.5Cu-0.1Zr-0.2Sc alloy after creep fracture, it can be observed that with the increase in applied stress, the precipitated phases undergo significant coarsening. It is generally believed that dispersed and uniformly fine precipitated phase particles can play a greater hindrance role in dislocation movement during the creep process, thereby reducing the creep rate of the alloy, while the hindrance of the coarsened second relative dislocation movement is greatly reduced. Therefore, the creep rate of the alloy increases.

The precipitate-free zone is usually considered to have an adverse effect on the mechanical properties of alloys, as dislocations in the precipitate-free zone are not hindered by the precipitate phase and their movement is easier. Moreover, the concentration of solute atoms in the precipitate-free zone is lower than that in other regions, and the degree of lattice distortion is relatively low. Therefore, the strengthening effect of the alloy is relatively weak compared to other regions. In summary, the movement of dislocations in the precipitate-free zone is less hindered, so the strength of the precipitate-free zone is much lower than that of other parts of the alloy, which affects the mechanical properties of the alloy. When the alloy is subjected to external stress, the non-precipitation zone area is more prone to stress concentration [20,21]. The width of the precipitate-free zone in the T6-state Al-6.5Zn-2.3Mg-2.5Cu-0.1Zr-0.2Sc alloy increases with the increase in applied stress. The width of the precipitate-free zone in the alloy under an applied stress of 180 MPa is much greater than that under 150 MPa. When the applied stress is 150 MPa, the widths of precipitate-free precipitation bands of the two aged alloys are not significantly different; when the applied stress is 180 MPa, the width of the precipitate-free zone in the 34 h aged alloy is significantly wider than that in the 22 h aged alloy. This explains why, when the applied stress is high, the creep lives of the two aged alloys differ significantly, while when the applied stress is low, the creep lives of the two aged alloys are very close.

## 5. Conclusions

1. At 200 °C, the tensile strength and yield strength of the alloy aged for 22 h were 617.7 MPa and 600.5 MPa, respectively; the tensile strength of the aged 34 h alloy was 575.9 MPa, and the yield strength was 560.7 MPa. The fracture mechanism of both alloys is ductile fracture.
2. The creep life of the Al-6.5Zn-2.3Mg-2.5Cu-0.1Zr-0.2Sc alloy in solid solution + aging state decreases and the steady-state creep rate increases with an increase in applied stress at 200 °C and 150–180 MPa stress conditions. The life of the 22 h aged alloy is higher than that of the 34 h aged alloy under different external stresses, and the creep deformation mechanism of both aged alloys is controlled by the precipitates.

**Author Contributions:** Conceptualization, W.Z.; methodology, Y.S.; software, Y.S. All authors have read and agreed to the published version of the manuscript.

**Funding:** This research received no external funding.

**Data Availability Statement:** Data are available in a publicly accessible repository.

**Conflicts of Interest:** The authors declare no conflict of interest.

## References

1. Wang, X.; Pan, Q.; Wang, W.; Huang, Z.; Chen, J.; Pan, B.; Liu, X. Effects of pre-strain and aging treatments on the mechanical property and corrosion resistance of the spray formed ultra-high strength Al-Zn-Mg-Cu alloy. *Mater. Charact.* **2022**, *194*, 112381. [CrossRef]
2. Zheng, G.Y.; Luo, X.; Kou, Z.D.; Huang, B.; Yang, Y.Q. Microstructural evolution of Al-Zn-Mg-Cu alloy during ultrasonic surface rolling process. *Mater. Charact.* **2022**, *194*, 112418. [CrossRef]
3. Parakh, A.; Lee, A.C.; Chariton, S.; Wang, M.M.; Kiani, M.T.; Prakapenka, V.B.; Gu, X.W. High-pressure deformation induced precipitation in Al–Zn–Mg–Cu alloy (Al7075). *Mater. Sci. Eng. A* **2022**, *853*, 143765. [CrossRef]
4. Bian, T.J.; Li, H.; Lei, C.; Wu, C.H.; Zhang, L.W. Microstructures and properties evolution of Al-Zn-Mg-Cu alloy under electrical pulse assisted creep aging. *Adv. Manuf.* **2022**, *10*, 596–609. [CrossRef]
5. Li, J.; He, Y.; Zhao, X.; Kim, C. Evolution of Microstructure and Mechanical Properties of Al-Zn-Mg-Cu Alloy by Extrusion and Heat Treatment. *Coatings* **2022**, *12*, 787. [CrossRef]
6. Shah, S.; Thronsen, E.; Hatzoglou, C.; Wenner, S.; Marioara, C.D.; Holmestad, R.; Holmedal, B. Effect of cyclic ageing on the early-stage clustering in Al–Zn–Mg(-Cu) alloys. *Mater. Sci. Eng. A* **2022**, *846*, 143280. [CrossRef]
7. Srivastava, V.; Williams, J.P.; McNee, K.R.; Greenwood, G.W.; Jones, H. Low stress creep behaviour of 7075 high strength aluminium alloy. *Mater. Sci. Eng. A* **2004**, *382*, 50–56. [CrossRef]
8. Peng, F.; Wang, J.; Yang, R.; Xia, Y.; Zhang, G.; Cai, B. Creep behavior and microstructural evolution of Al-Cu-Mg-Ag alloys with various high Cu contents. *Metals* **2021**, *11*, 487. [CrossRef]
9. Lin, Y.C.; Xia, Y.C.; Ma, X.S.; Jiang, Y.Q.; Chen, M.S. High-temperature creep behavior of Al-Cu-Mg alloy. *Mater. Sci. Eng. A* **2012**, *550*, 125–130. [CrossRef]
10. Xu, Y.; Zhan, L.; Huang, M.; Shen, R.; Ma, Z.; Xu, L.; Wang, K.; Wang, X. Deformation behavior of Al-Cu-Mg alloy during non-isothermal creep age forming process. *J. Mater. Process. Technol.* **2018**, *255*, 26. [CrossRef]
11. Xu, Y.; Zhan, L.; Xu, L.; Huang, M. Experimental research on creep aging behavior of Al-Cu-Mg alloy with tensile and compressive stresses. *Mater. Sci. Eng. A* **2017**, *688*, 488. [CrossRef]
12. Wang, Y.C.; Wu, X.D.; Lu, Y.U.E.; Guo, M.X.; Cao, L.F. Aging precipitation behavior and properties of Al–Zn–Mg–Cu–Zr–Er alloy at different quenching rates. *Trans. Nonferrous Met. Soc. China* **2022**, *32*, 1070–1082. [CrossRef]
13. Chasse, K.R.; Rajendran, R.; Owens, C.T.; Singh, P.M. Stress Corrosion Cracking Susceptibility of Additively Manufactured Aluminum Alloy 7050 Produced by Selective Laser Melting in Chloride Environments. *J. Mater. Eng. Perform.* **2021**, *30*, 7046–7056. [CrossRef]
14. Kang, K.; Li, D.; Shi, D.; Gao, G.; Xu, Z.; Wang, L. Evolution of Microstructure and Mechanical Properties in Al–Zn–Mg–Cu Alloy by Electric Pulse Aging Treatment. *Trans. Indian Inst. Met.* **2021**, *74*, 2835–2842. [CrossRef]
15. Moshtaghi, M.; Safyari, M.; Hojo, T. Effect of solution treatment temperature on grain boundary composition and environmental hydrogen embrittlement of an Al–Zn–Mg–Cu alloy. *Vacuum* **2021**, *184*, 109937. [CrossRef]
16. Moon, C.; Thuillier, S.; Lee, J.; Lee, M.G. Mechanical properties of solution heat treated Al-Zn-Mg-Cu (7075) alloy under different cooling conditions: Analysis with full field measurement and finite element modeling. *J. Alloys Compd.* **2021**, *856*, 158180. [CrossRef]
17. Lee, S.H.; Jung, J.G.; Baik, S.I.; Seidman, D.N.; Kim, M.S.; Lee, Y.K.; Euh, K. Precipitation strengthening in naturally aged Al-Zn-Mg-Cu alloy. *Mater. Sci. Eng. A* **2020**, *803*, 140719. [CrossRef]
18. Wen, K.; Xiong, B.Q.; Zhang, Y.A.; Li, X.W.; Li, Z.H.; Yan, L.Z.; Yan, H.W.; Liu, H.W. Aging precipitation characteristics and tensile properties of Al-Zn-Mg-Cu alloys with different additional Zn contents. *Rare Met.* **2020**, *40*, 2160–2166. [CrossRef]
19. Li, L.; Li, R.; Yuan, T.; Chen, C.; Zhang, Z.; Li, X. Microstructures and tensile properties of a selective laser melted Al-Zn-Mg-Cu alloy by Si and Zr microalloying. *Mater. Sci. Eng. A* **2020**, *787*, 139492. [CrossRef]
20. Lei, C.; Yang, H.; Li, H.; Shi, N.; Fu, J.; Zhan, L. Dependence of creep age formability on initial temper of an Al-Zn-Mg-Cu alloy. *Chin. J. Aeronaut.* **2016**, *29*, 1445–1454. [CrossRef]
21. Zhang, J.; Wang, Y.; Deng, Y.; Zhang, X. Effect of deformation degree on the creep age forming of 7475 aluminum alloy: The feasibility of the extended deformation range. *Mater. Sci. Eng. A* **2016**, *664*, 126–134. [CrossRef]